Sādhanā Vol. 40, Part 7, October 2015, pp. 2045–2072. © Indian Academy of Sciences

Computationally efficient models for simulation of non-ideal DC–DC converters operating in continuous and discontinuous conduction modes

CHALLA MOHANA KRISHNA*, SARITHA B and NARAYANAN G

Department of Electrical Engineering, Indian Institute of Science Bangalore, Bangalore 560012, India
e-mail: mohankrishnachalla@gmail.com

MS received 30 September 2014; revised 9 April 2015; accepted 19 July 2015

Abstract. This paper discusses dynamic modeling of non-isolated DC–DC converters (buck, boost and buck–boost) under continuous and discontinuous modes of operation. Three types of models are presented for each converter, namely, switching model, average model and harmonic model. These models include significant non-idealities of the converters. The switching model gives the instantaneous currents and voltages of the converter. The average model provides the ripple-free currents and voltages, averaged over a switching cycle. The harmonic model gives the peak to peak values of ripple in currents and voltages. The validity of all these models is established by comparing the simulation results with the experimental results from laboratory prototypes, at different steady state and transient conditions. Simulation based on a combination of average and harmonic models is shown to provide all relevant information as obtained from the switching model, while consuming less computation time than the latter.

Keywords. Average model; buck converter; boost converter; buck–boost converter; harmonic model; switching model.

1. Introduction

DC–DC converters are an integral part of many modern electrical applications such as electric/hybrid electric vehicles (Khan 1994; Bellur *et al* 2007) and on-board ship power systems (Zahedi & Norum 2013). To ensure good performance of such complex electrical system, various electrical components of the system are to be designed, controlled and integrated appropriately. Modeling and simulation of various components help to minimize the time and cost of development of the individual sub-systems as well as the overall system (Williamson *et al* 2006; Emadi *et al* 2006).

*For correspondence

Both off-line and real-time simulation can be used to analyze the feasibility, stability and performance of the electrical system. However, off-line simulation is a priori to real-time simulation. In this paper, the models of various non-ideal converters are analyzed under off-line simulation environment. Conventionally, non-idealities of the converters are ignored during modeling (Fang 2011). This paper discusses the development of the average, harmonic and switching models of the non-isolated non-ideal DC–DC converters (Buck, Boost and Buck–Boost).

In an electric vehicle, the DC–DC converters are operated at high switching frequencies to reduce the rating and size of the passive components (Waffler & Kolar 2009). To simulate a switching model of the converter, the time step for the simulation must be very small compared to the switching period of the active switches in the converter. Reducing the simulation time step increases the computation time and the memory resource consumption (Patil *et al* 2009).

Averaging techniques, discussed in literature (Pedicini *et al* 2012; Krein *et al* 1989; Sanders *et al* 1990; Lehman & Bass 1994; Ren *et al* 2000; Jalla *et al* 2004; Chung *et al* 2009), include state-space and switching cycle averaging methods. State-space averaging technique is a matrix based technique, increasing the computational effort (Vuthchhay & Bunlaksananusorn 2008). Hence the switching-cycle-averaged model is used in this paper.

Average models of dc–dc converters yield the voltages and currents of the converter, averaged over each switching cycle. The simulated voltage and current waveforms contain only the dc and low-frequency components, and not the switching-frequency ripple. Prediction of such switching-cycle-averaged waveforms is sufficient in many practical situations. More importantly, simulation with such an average model consumes much less time than the switching model since the time step could be much longer than in case of a switching model.

Most average models of dc–dc converters are valid for converter operation with moderate to heavy loads, when the converter is operating in the so-called continuous conduction mode (CCM) (Merdassi *et al* 2008). A few models pertain only to light load conditions or the so-called discontinuous conduction mode (DCM) (Hwang & Park 2012). The models presented in this paper can predict the operation of the converter under heavy loads (i.e. CCM), light loads (i.e. DCM) and also during transition between light and heavy loads.

While prediction of average voltages and currents is sufficient under many scenarios, ripple quantities are also important for the converter design. The ripple on output voltage, for example, is an important design specification, indicating the quality of the converter output (Mohan *et al* 2007). The sizing of the filter components depend on the maximum allowable ripple currents and voltages in the converter (Badstuebner *et al* 2010). Further, the ripple quantities also determine or influence the losses in various components. Hence this paper presents the harmonic model for each of the dc–dc converters to evaluate the peak-to-peak voltage and current ripples, based on certain average voltages and currents in the converter. It is shown that a combination of average model and harmonic model, termed here as combined model, can give all the essential information that are available from the switching model.

The authors presented the preliminary results pertaining to the non-ideal boost converter in the National Power Electronics Conference (NPEC) (Saritha *et al* 2013). This paper presents and evaluates the switching model, average model, harmonic model and combined model for non-ideal buck, boost and buck–boost converters, in detail. The models are evaluated in terms of accuracy and computational effort. The accuracy of the models is verified by comparing the simulation results with the experimental data from 20 W laboratory prototype converters. The models are compared in terms of computational time required for simulation of the converters in MATLAB environment.

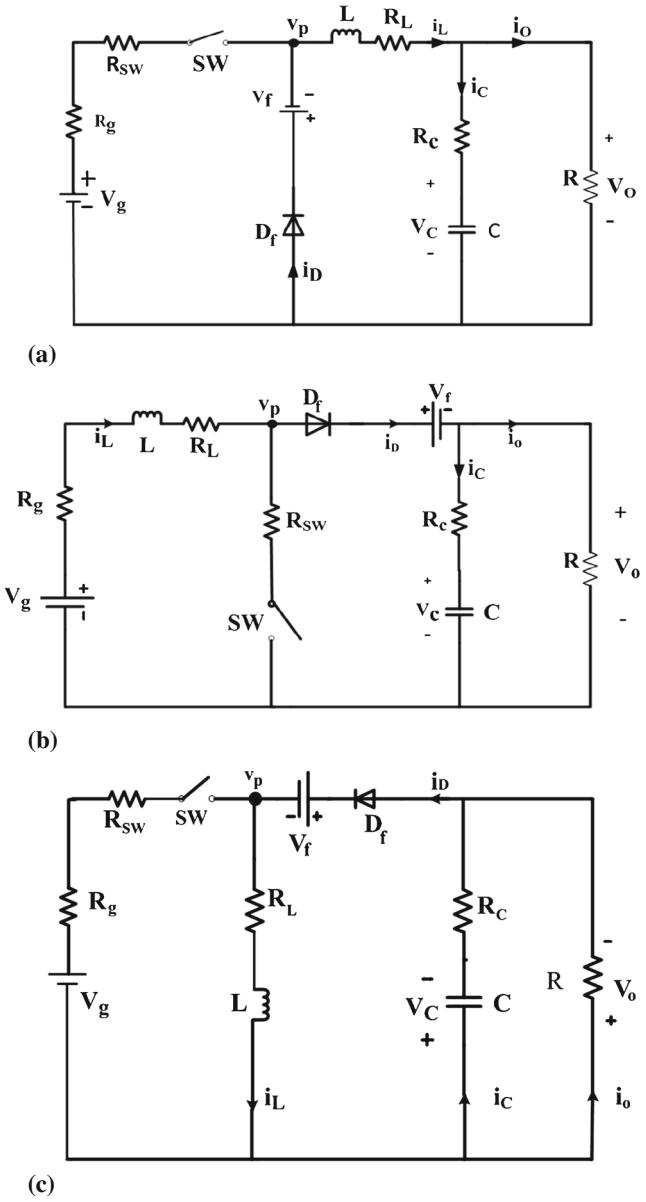

Figure 1. Circuit schematic of non-ideal (**a**) buck converter (**b**) boost converter (**c**) buck–boost converter.

2. Approach to modeling of non-ideal DC–DC converterss

A buck converter, a boost converter and a buck–boost converter having significant non-idealities are shown schematically in figures 1(a), 1(b) and 1(c), respectively. There are both similarities and dissimilarities among the three converters. This section presents an approach to modeling of non-ideal dc–dc converters.

2.1 *Non-idealities*

The non-ideal voltage source (or the output of the previous power conversion stage) is denoted by a voltage source with an open-circuit voltage V_g and an internal resistance R_g. Each non-ideal active and passive element in the converter is represented by an ideal element in series with a resistance, which is a quantitative representation of the non-ideality. The actual MOSFET is represented as an ideal switch SW in series with the on-state drain-to-source resistance R_{SW}, and the diode is considered as an ideal diode D_f in series with a forward voltage drop V_f. The practical inductor is represented as a series combination of inductance L and resistance R_L. The non-ideal capacitor is regarded as a combination of an ideal capacitor C with an equivalent series resistance R_C. The load or the next power conversion stage is modeled as a resistance R.

For simulation and experimental validation of the models of the three converters, the converter parameters considered are as shown in table 1. Both the values of the ideal elements and also their respective non-idealities in the three converters are tabulated in table 1.

2.2 *Switching functions*

The status of the ideal switch SW and that of the diode D_f are given by the switching functions S_1 and S_2, respectively. The switching function is either 1 or 0, depending on whether the device is ON or OFF. The switching function S_1 is supplied by the controller, and S_2 is generated by the converter model. The average values of S_1 and S_2 over a switching cycle are the duty ratio of MOSFET (i.e. D_1) and that of diode (i.e. D_2), respectively. Similar to S_1 and S_2, the duty ratio D_1 is an input to the converter model, and D_2 is generated internally by the model.

2.3 *Conduction modes*

In all the three dc–dc converters, energy gets stored into the inductor during the ON-time of the active switch (MOSFET). The energy stored at the end of the ON-time causes freewheeling of the inductor current through the diode. If the energy stored is high enough, then the freewheeling action or conduction through the inductor continues throughout the OFF-time of the active switch, as illustrated in figure 2(a). This is termed as continuous conduction mode (CCM). On the other hand, if the energy stored is inadequate, the current conduction through the inductor and diode stops midway through the OFF-time of the active switch, as shown in figure 2(b). This is termed as discontinuous conduction mode (DCM). During the ON-time of MOSFET, the switching functions are $S_1 = 1$ and $S_2 = 0$. When the freewheeling diode is ON, the switching functions are $S_1 = 0$ and $S_2 = 1$. In case of DCM, when both the MOSFET and diode are OFF, the switching functions are $S_1 = 0$ and $S_2 = 0$.

Table 1. Value of the various components in dc–dc converter.

Components of the converter	Buck converter	Boost converter	Buck–Boost converter
Inductor (L)	12.5 mH	2 mH	2.5 mH
Capacitor (C)	22 μF	11 μF	10 μF
Load (R)	25 Ω	100 Ω	222 Ω
Drop across diode (V_f)	0.8 V	0.8 V	0.8 V
ON resistance of switch (R_{sw})	55 mΩ	55 mΩ	55 mΩ
Resistance of inductor (R_l)	2.5 Ω	2 Ω	3.5 Ω
Series resistance of capacitor (R_c)	1.5 Ω	3 Ω	0.61 Ω
Source resistance (R_{in})	1 m Ω	1 m Ω	1 m Ω

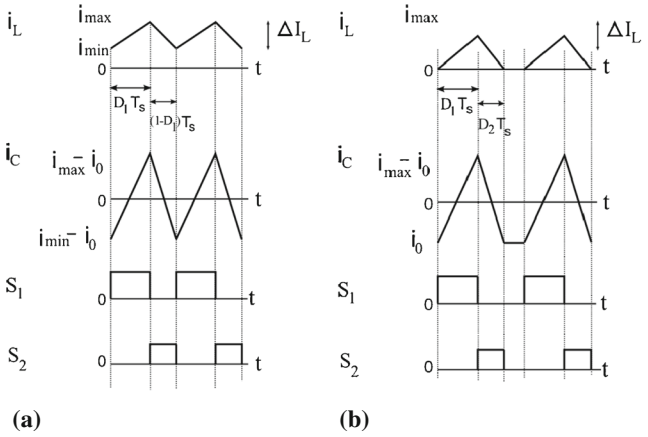

Figure 2. Inductor current under (**a**) CCM (**b**) DCM.

2.4 *Pole voltage*

The common node between the active device and the diode is termed as *pole*. Each of the three converters can be seen as a second-order system, driven by the pole voltage (v_p) as an input. It is straightforward to express the pole voltage in terms of the input voltage V_g and switching functions in an ideal dc–dc converter. This paper presents a generalized pole voltage expression for each converter, valid for both CCM and DCM, and inclusive of the effects of non-idealities.

2.5 *Inductor current*

The voltage at one terminal of the inductor L in a DC–DC converter (buck or boost or buck–boost) is fixed. This may be the input voltage, the output voltage or the reference zero. Hence the inductor current is controlled by the pole voltage v_p, which is applied at the other terminal of the inductor. Essentially, the difference between the pole voltage on one terminal and the fixed voltage on the other terminal, is integrated to calculate inductor current i_L.

2.6 *Output voltage*

The capacitor current i_C is essentially the ripple component of the inductor current i_L (in case of buck converter) or that of the diode current i_D (in case of boost and buck–boost converters). In the latter case, the diode current i_D is obtained by multiplying the inductor current i_L with the switching function S_2. The load current i_0 is subtracted from i_L or i_D, to determine its ripple component i.e. i_C. The capacitor voltage v_c is obtained by integration of the capacitor current i_C. The output voltage v_0 is the sum of capacitor voltage v_c and the voltage drop across the equivalent series resistance (ESR) of the capacitor R_C.

2.7 *Types of dynamic models*

The modeling approach, discussed so far, is represented by the block diagrams in figure 3. Dynamic modeling of a converter can provide either the instantaneous values (switching model)

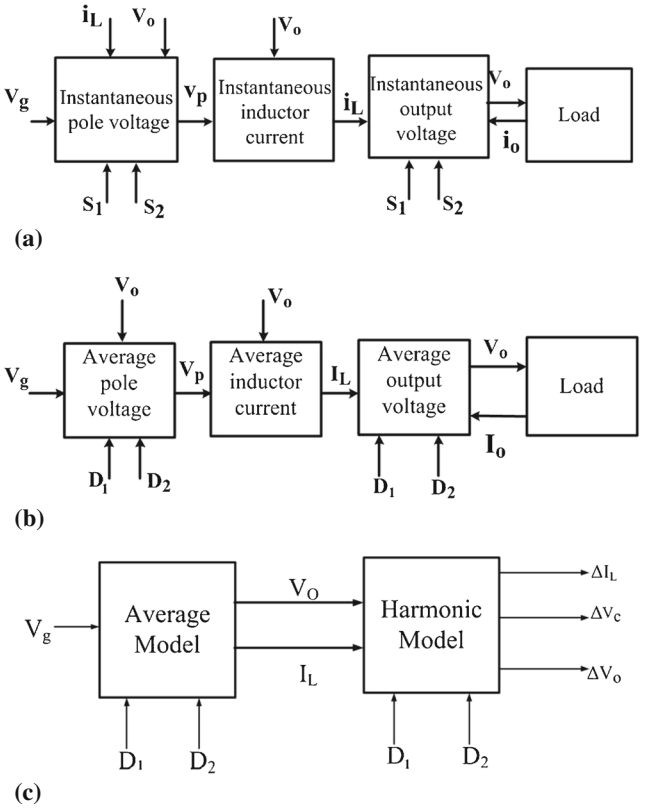

Figure 3. General representation of the models of converter (**a**) switching model (**b**) average model (**c**) combined average and harmonic model.

or the switching-cycle averaged values (average model) of the electrical quantities. As seen from figure 3(a), the switching model is driven by the switching functions S_1 and S_2. Using the switching functions and the input voltage, the instantaneous pole voltage v_p is generated, which is then used to evaluate the inductor current and output voltage. The average model, shown in figure 3b, is driven by the duty cycles D_1 and D_2. This model produces the average pole voltage V_P; the average inductor current I_L and average output voltage V_0 are calculated from V_P. These average quantities, along with the two duty ratios, are used by the harmonic model to evaluate the peak-to-peak ripple in inductor current (ΔI_L) and that in output voltage (ΔV_o), as shown by figure 3(c). The average model and the harmonic model in cascade, as shown by figure 3(c), are termed as the combined model, in this paper.

3. Switching model

The switching models of the buck, boost and buck–boost converters are shown by figures 4(a), 4(b) and 4(c), respectively. These switching models can mimic the behavior of the converters under CCM as well as DCM. The switching function S_1 of an ideal switch SW is supplied by the

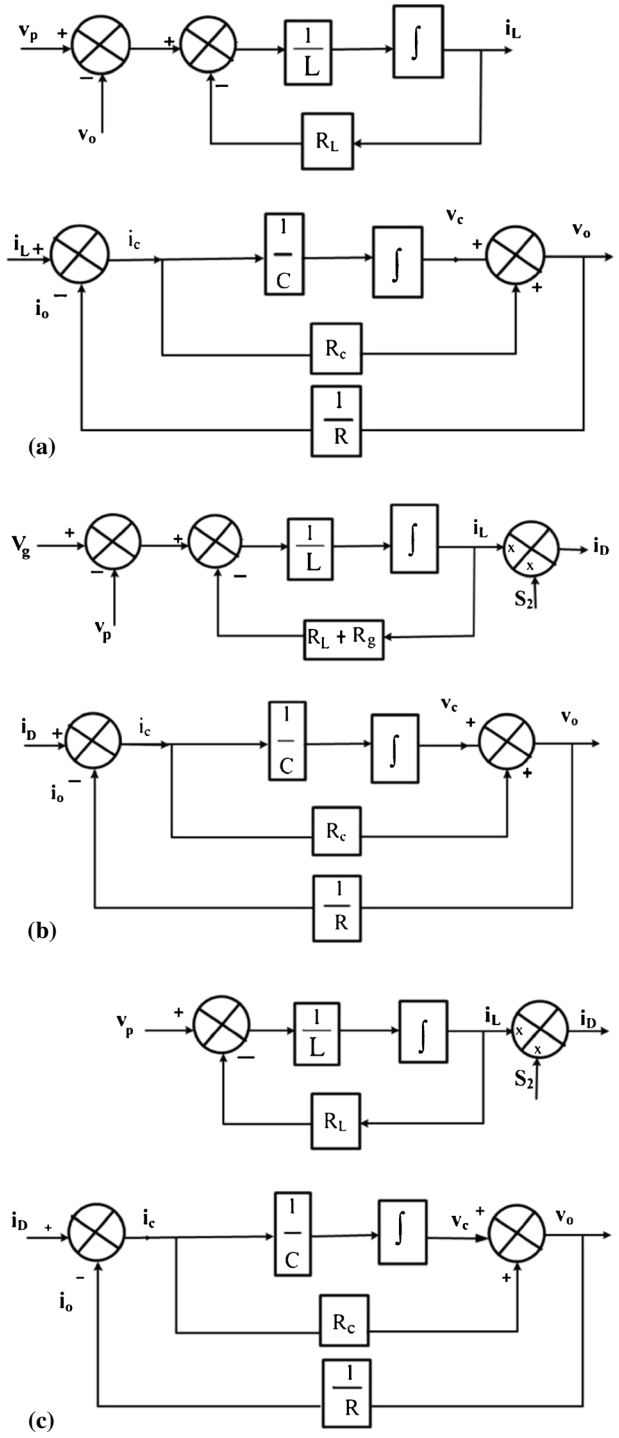

Figure 4. Block diagram representation of the model of (**a**) buck converter (**b**) boost converter (**c**) buck–boost converter.

Table 2. Expression for instantaneous pole voltage v_p for different converters.

Converter	Mode	Voltage v_p
Buck	CCM	$(v_g - i_L R_g - R_L i_L)S_1 - (V_f)S_2$
	DCM	$(v_g - i_L R_g - R_L i_L)S_1\overline{S_2} - (V_f)\overline{S_1}S_2 + V_o\overline{S_1}\,\overline{S_2}$
Boost	CCM	$i_L R_{sw}S_1 + (v_o + V_f)S_2$
	DCM	$i_L R_{sw}S_1\overline{S_2} + (v_o + V_f)\overline{S_1}S_2 + Vg\overline{S_1}\,\overline{S_2}$
Buck–Boost	CCM	$(V_g - i_L R_g - R_{SW} i_L)S_1 + (-v_o - V_f)S_2$
	DCM	$(V_g - i_L R_g - R_{SW} i_L)S_1\overline{S_2} + (-v_o - V_f)\overline{S_1}\,S_2$

controller. The function S_2 is generated within simulation program as shown by the following equation.

$$\begin{aligned} S_2 &= \overline{S_1} \quad \text{if } i_L > 0 \\ &= 0 \quad \text{if } i_L = 0. \end{aligned} \tag{1}$$

The switching functions are used to determine the instantaneous pole voltage v_P. The expressions for v_P are different for the three converters, as shown by table 2. These equations are obtained from the respective schematic diagrams of the converters, shown in figure 1. It can be seen that the expression for v_P under DCM is more general and is used in the simulation of a switching model. By imposing $S_2 = \overline{S_1}$ on the general expression, the corresponding expression for CCM operation is obtained.

Calculation of inductor current i_L based on v_P and output voltage v_o based on i_L are illustrated by the block diagram in figure 4(a), which together with Eq. (1), define the switching model of a buck converter. In figures 4(b) and 4(c), the inductor current i_L is multiplied by the switching function S_2 to obtain the diode current i_D. The diode current i_D is then used to calculate the capacitor voltage v_c and the output voltage v_o of the boost and buck–boost converters.

4. Average model

Averaged model provides ripple free averaged values of various voltages and currents of the converter. The non-idealities in the converter could have significant effect on the output voltage. Expressions are derived in this section for the output voltage of the non-ideal converters. The output voltage depends not only on the duty ratio of the MOSFET, but also on that of the diode. Hence expressions are derived for the duty ratio of the diode (i.e. D_2) for the three converters. These are used to determine the boundary conditions for CCM and DCM operation of the converters.

4.1 *Non-ideal voltage gain*

Referring to figure 1(a), the volt-second balance across the ideal inductance L in a buck converter at steady state can be expressed as shown in (2). Further, this equation can be rewritten as shown in (3), where $I_{L,ON}$ and $I_{L,OFF}$ are the average values of the inductor current over the on-time and off-time, respectively, of the MOSFET switch.

$$\int_0^{D_1 T_s} (V_g - i_L(R_g + R_{sw} + R_L) - V_0)\mathrm{d}t = \int_{D_1 T_s}^{(D_1+D_2)T_s} (V_f + i_L R_L + V_0)\mathrm{d}t \tag{2}$$

$$(V_g - I_{L,ON}(R_g + R_{sw} + R_L) - V_0)D_1T_s = (V_f + I_{L,OFF}R_L + V_0)D_2T_s \tag{3}$$

$$I_{L,ON} = \frac{I_p}{2}; I_{L,OFF}\frac{I_p}{2} \text{ and } I_p = \frac{2V_0}{R}\frac{1}{D_1 + D_2}. \tag{4}$$

During the on-time of the MOSFET, the time constant $\tau_{ON} = \frac{L}{(R_g+R_{SW}+R_L)}$ is much longer than the on-time of the switch i.e. D_1T_S. Similarly, during the off-interval of the active switch, the time constant $\tau_{OFF} = \frac{L}{(R_L)}$ is very much high, compared to D_2T_S. Hence the inductor current can be assumed to vary linearly with time in both the intervals as shown in figure 2. Consequently, $I_{L,ON}$ and $I_{L,OFF}$ can be expressed in terms of the peak current i_P as shown in (4). The peak current is also related to the output voltage V_o, as shown in (4).

Using (3) and (4), the non-ideal output voltage V_0 of the buck converter can be expressed in terms of V_g, D_1 and D_2 as shown in table 3. A similar procedure is followed to derive the expressions for V_0 for the boost and buck–boost converters. These expressions are also tabulated in table 3. All these expressions pertain to the more general case of DCM. Replacing the variable D_2 by $(1-D_1)$ in these expressions yields the output voltage pertaining to CCM operation of the converters.

4.2 *Calculation of duty ratio D_2*

Considering DCM, the KVL equation of the inductive circuit during the diode conduction period D_2T_s in a non-ideal buck converter can be written, as shown in (5). The corresponding averaged KVL equation is shown in (6). The average inductor current during the off-time of the switch $I_{L,OFF}$ and peak current I_p are expressed in terms of output voltage V_0, as shown in (7).

$$L\frac{di_L}{dt} = V_f + V_0 + i_L R_L \tag{5}$$

$$L\frac{I_p}{D_2T_s} = V_f + V_0 + I_{L,OFF}R_L \tag{6}$$

$$L\frac{2V_0}{R}\frac{1}{D_1 + D_2}\frac{1}{D_2T_s} = V_f + V_0 + \frac{V_0}{R}\frac{1}{D_1 + D_2}R_L \tag{7}$$

Substituting for the output voltage V_o in (7) by the appropriate expression from table 3, an equation is obtained, which relates D_1 and D_2 in a buck converter. This equation is

Table 3. Steady-state output voltage of the non-ideal converters.

Type	Voltage V_0
Buck	$\frac{V_gD_1 - V_fD_2}{\frac{R_L}{R} + \frac{D_1}{(D_1+D_2)}\frac{(R_g+R_{SW})}{R} + D_1 + D_2}$
Boost	$\frac{V_g(D_2^2 + D_1D_2) - V_fD_2^2}{\frac{(R_g+R_L+R_{SW})}{R}D_1 + D_2\frac{(R_g+R_L)}{R} + D_2^2}$
Buck–Boost	$-\left[\frac{V_gD_1 + V_fD_2}{D_2 + \frac{R_L}{R} - \frac{D_1}{D_2}\left(\frac{R_g+R_L+R_{SW}}{R}\right)}\right]$

Table 4. Expression for D_2 including non-idealities.

Converter	Expression for D_2
Buck	$D_2^3 V_f - D_1 D_2^2 V_g + D_2 \left(-K V_f - D_1^2 V_g - 2D_1^2 V_f - \frac{R_L}{R} D_1 V_f\right) + \left(D_1 V_g K - D_1^3 V_f - D_1^2 \frac{R_g + R_{SW}}{R} V_f - \frac{R_L}{R} D_1^2 V_f\right) = 0$
Boost	$D_1 D_2^2 - K \left(1 - \frac{V_f}{V_g}\right) D_2 + \frac{V_f}{V_g} \frac{R_g + R_L + R_{SW}}{R} D_1 - \frac{R_{SW}}{R} D_1 D_2 - K D_1 = 0$
Buck–Boost	$D_1 D_2^2 + \left(\frac{R_L}{R} D_1 - K \frac{V_f}{V_g} + \frac{V_f}{V_g} D_1 \frac{R_g + R_L + R_{SW}}{R}\right) D_2 - K D_1 = 0$

shown in table 4, where K is termed as the conduction parameter, and is given by the following equation:

$$K = \frac{2L}{RT_s}. \tag{8}$$

Similar equations for the other two converters are also shown in table 4. These equations are used to calculate D_2, with knowledge of D_1. Under CCM, D_2 is calculated as $(1-D_1)$.

4.3 *Impact of non-idealities on diode duty ratio D_2 and output voltage*

The variations of D_2 with duty cycle D_1 for the non-ideal buck, boost and buck–boost converters are plotted in figures 5(a), 5(b) and 5(c), respectively. The corresponding variations are also plotted, ignoring the non-idealities, on the same figures. It can be inferred from figure 5 that the change in D_2 on account of the non-idealities is not very significant, at least for the sets of parameters considered in this paper. Hence, the non-idealities could be ignored, and the simplified expressions as given in table 5 could be considered for the evaluation of D_2. Under CCM, D_2 is calculated as $(1-D_1)$.

However, the non-idealities have significant effect on the average output voltage as shown in table 6, which compares the ideal output voltage (ignoring the non-idealities) and the actual output voltages (considering the non-idealities) of the dc–dc converters at different operating conditions.

4.4 *Boundary condition between CCM and DCM*

At the boundary between the continuous and discontinuous condition modes of any converter, the duty ratios D_1 and D_2 are related as follows:

$$D_2 = (1 - D_1). \tag{9}$$

This substitution can be made in the equations relating D_1 and D_2 in table 4, which considers the non-idealities. The value of K at this boundary condition is termed as critical conduction parameter K_{cri}. The expressions for K_{cri} for the three non-ideal converters are shown in table 7. If the conduction parameter K, defined in (8), is greater than K_{cri}, then the operation is in CCM as indicated by (10); otherwise the operation is in DCM as indicated by (11).

$$K > K_{cri} \quad \text{for CCM} \tag{10}$$

$$K < K_{cri} \quad \text{for DCM}. \tag{11}$$

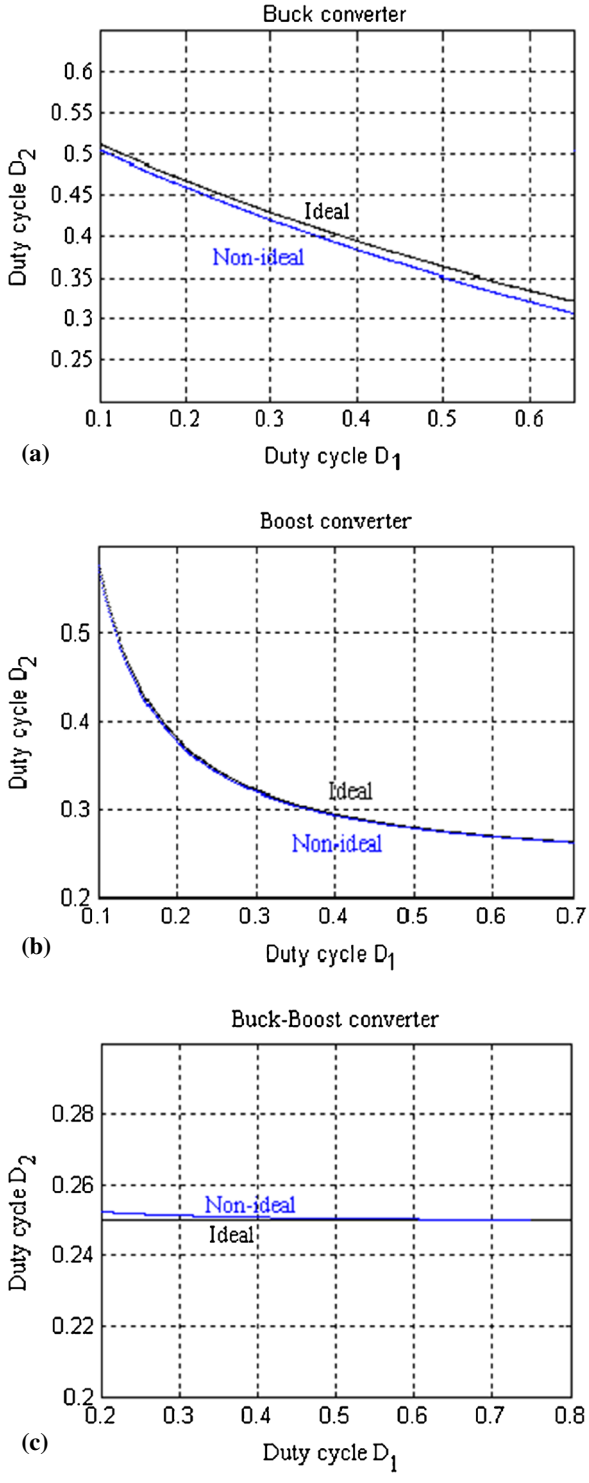

Figure 5. Variation of D_2 with D_1 for (**a**) buck (**b**) boost (**c**) buck–boost converter.

Table 5. Calculation of duty cycle D_2 under DCM ignoring non-idealities.

Converter	D_2
Buck	$\frac{-D_1+\sqrt{D_1^2+4K}}{2}$
Boost	$\frac{K+\sqrt{K^2+4D_1^2K}}{2D_1}$
Buck–Boost	$\sqrt{K}$

Table 6. Comparison of ideal and non-ideal output voltage of dc–dc converters.

Converter type	Input voltage V_g	Duty ratio D_1	Mode	Load R (Ω)	Switching frequency f_s (kHz)	Ideal output voltage	Non-ideal output voltage
Buck	40	0.5	CCM	200	20	20	19.4
	40	0.15	DCM	2,000	20	10.3	9.9
	20	0.15	DCM	2,000	20	28	27.3
Buck–Boost	20	0.5	CCM	200	20	20	17.83
	20	0.15	DCM	1,000	20	9.49	8.97

Table 7. Value of K_{cri} for various non-ideal dc–dc converters.

Type	Critical conduction parameter K_{cri}
Buck	$\frac{D_1^2\left(V_g+V_f-\frac{(R_g+R_{SW})}{R}V_f\right)-D_1\left(V_g+\frac{R_L}{R}V_f+3V_f\right)+V_f}{V_f(1-D_1)-D_1V_g}$
Boost	$\frac{D_1^3+D_1^2\left(\frac{R_{SW}}{R}-2\right)+D_1\left(1-\frac{R_{SW}}{R}+\frac{V_f}{V_g}\left(\frac{R_g+R_L+R_{SW}}{R}\right)\right)}{1-\frac{V_f}{V_g}(1-D_1)}$
Buck–Boost	$\frac{D_1^3+D_1^2\left(-2-\frac{R_L}{R}-\frac{V_f}{V_g}\frac{(R_g+R_L+R_{SW})}{R}\right)+D_1\left(1+\frac{R_L}{R}\frac{V_f}{V_g}\frac{(R_g+R_L+R_{SW})}{R}\right)}{D_1+\frac{V_f}{V_g(1-D_1)}}$

However, since D_2 is shown not to vary significantly due to the non-idealities, the simplified expressions for D_2 in table 5 can be used. Equating these expressions to $(1-D_1)$, much simplified expressions are obtained for K_{cri} as shown in (12)–(14).

$$K_{cri} = 1 - D_1; \quad \text{Buck} \tag{12}$$

$$K_{cri} = D_1(1 - D_1)^2; \text{Boost} \tag{13}$$

$$K_{cri} = (1 - D_1)^2; \text{Buck–Boost}. \tag{14}$$

Table 8. Averaged value of V_p and I_D of the converters.

Type of converter	Variable	Value
Buck	V_p	$\left(V_g - \frac{I_L}{D_1+D_2}\left(R_g + R_{SW}\right)\right) D_1 - (V_f) D_2 + V_0(1 - D_1 - D_2)$
Boost	V_p	$\frac{I_L}{D_1+D_2} R_{SW} D_1 + \{(V_0 + V_f)\, D_2\} + V_g(1 - D_1 - D_2)$
	I_D	$I_L \dfrac{D_2}{D + D_2}$
Buck–Boost	V_p	$\left(V_g - \left(R_g + R_{SW}\right) \frac{I_L}{D_1+D_2}\right) D_1 + (-V_0 - V_f) D_2$
	I_D	$I_L \dfrac{D_2}{D_1 + D_2}$

4.5 *Dynamic average modeling*

The dynamic average modeling of the converters is represented by the block diagram in figure 3b. The average pole voltage V_p is determined using the input voltage V_g, duty cycle D_1 and diode duty cycle D_2 as indicated in the figure. Table 8 shows the expressions for V_P used in the average models of the three converters. The average pole voltage V_p is used to evaluate the average inductor current I_L as mentioned earlier. The relation between the average inductor current I_L and the average diode current I_D is also shown for the boost and buck–boost converters in the same table. The average diode current is used to determine the average capacitor voltage and average output voltage as shown in figure 3(b).

5. Harmonic model

The value of peak to peak ripple in various currents and voltages of the converter is given by the harmonic model. The ripple in inductor current (ΔI_L), capacitor voltage (ΔV_C) and output voltage (ΔV_0) are provided by the harmonic model, using the results from the average model of the converter, as shown in figure 3c. The harmonic model of various converters is discussed in the following sections.

5.1 *Harmonic model of buck converter*

In buck converter, shown in figure 1(a), the average inductor current (I_L) is equal to the load current (I_0). The ripple in inductor current (ΔI_L) passes through the capacitor (ΔI_c) i.e. $\Delta I_C = \Delta I_L$. Under CCM, the inductor current i_L is continuous and is plotted in figure 6(a). The ripple component of i_L (i.e. i_L–i_0) flows through the capacitor, as shown in figure 6(b). The integral of capacitor current, divided by the capacitance C, gives the value of capacitor ripple voltage (ΔV_C) (figure 6(c)). The drop across the series resistance (R_c) of the capacitor has the same shape as that of capacitor current. The sum of drop across R_c and the voltage ripple across C gives the value of output voltage ripple (ΔV_o), as shown in figure 6(d).

Under DCM, the inductor current is zero during certain interval in the switching cycle, as shown in figure 7(a). The capacitor current under DCM operation is shown in figure 7(b). The capacitor ripple voltage and output voltage ripple are plotted in figure 7(c) and 7(d) respectively.

The value of inductor ripple current is calculated from the voltage across the inductor during ON or OFF period of the switch. The value of ΔI_L under CCM/DCM operation of buck converter

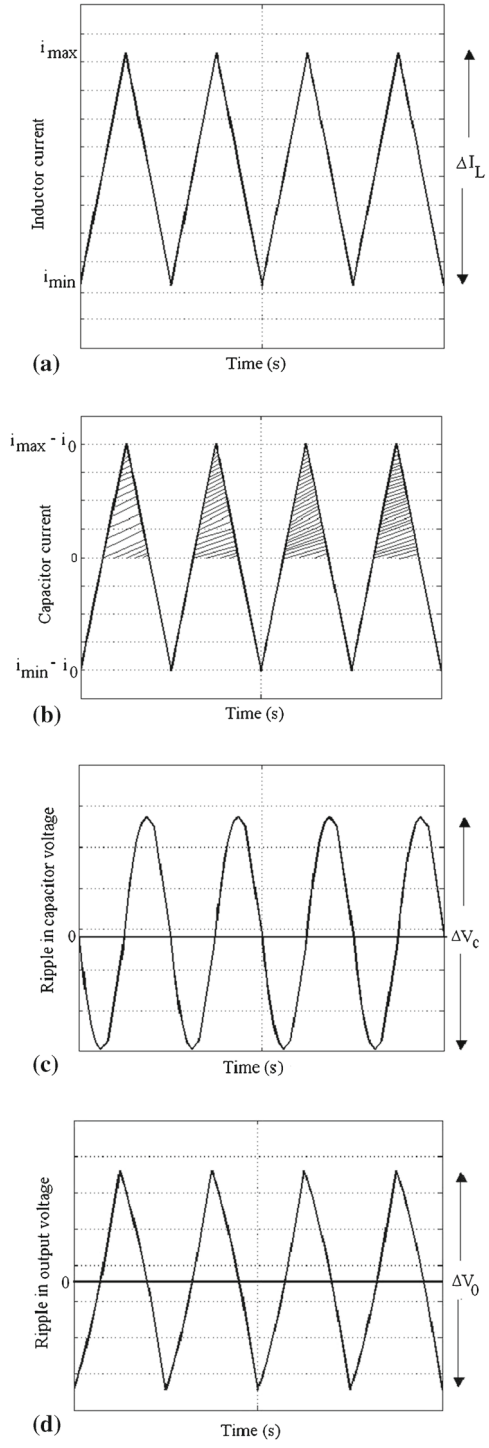

Figure 6. Buck converter under CCM (**a**) inductor current (**b**) capacitor current (**c**) capacitor voltage (**d**) output voltage.

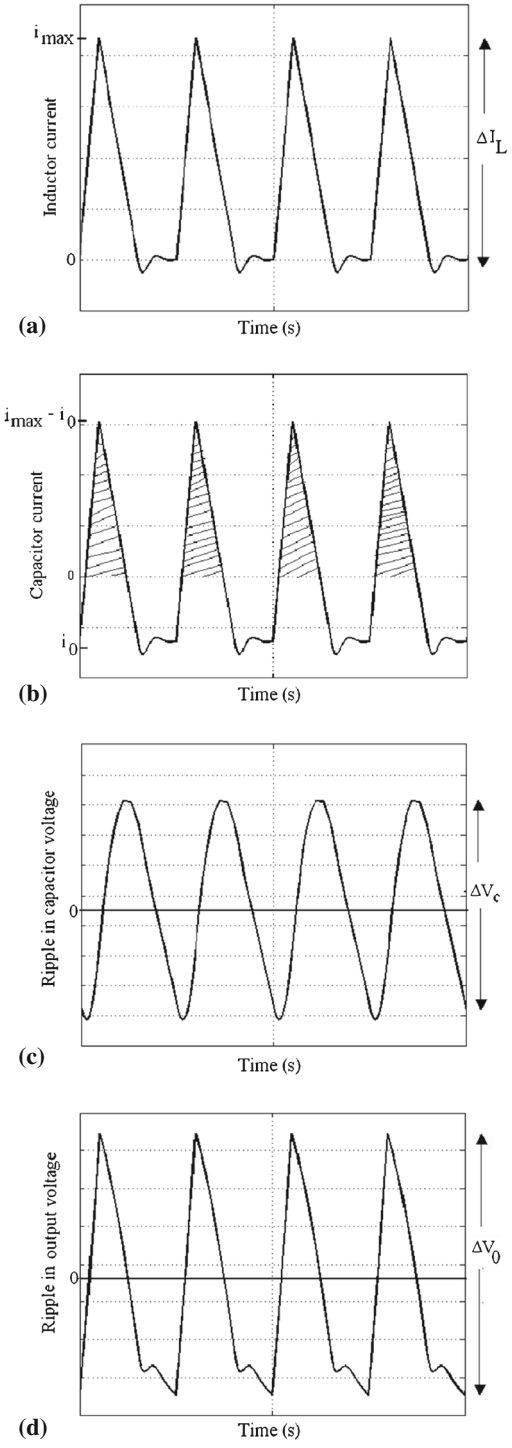

Figure 7. Buck converter under DCM (**a**) inductor current (**b**) capacitor current (**c**) ripple in capacitor voltage (**d**) ripple in output voltage.

Table 9. Output of harmonic model of buck converter.

Variable	Operation mode	
	CCM	DCM
ΔI_L	$\frac{(I_L R_L + V_o + V_f) * (1 - D_1) T_S}{L}$	$\frac{(I_L R_L + V_o + V_f) * D_2 T_S}{L}$
ΔV_C	$\frac{\Delta I_L T_S}{8C}$	$\frac{(D_1 + D_2) T_s (\Delta I_L - I_o)^2}{2C \Delta I_L}$

Table 10. Output of harmonic model of Boost and Buck–Boost converters.

Variable	Operation mode	
	CCM	DCM
ΔI_L	$\frac{(V_g - I_L(R_g + R_{sw} + R_L)) D_1 T_s}{L}$	$\frac{(V_g - I_L(R_g + R_{sw} + R_L)) D_1 T_s}{L}$
ΔV_C ($I_o < I_{min}$)	$\frac{V_0 D_1 T_s}{RC}$	$\frac{D_2 T_S (I_{max} - I_o)^2}{2C I_{max}}$
ΔV_C ($I_o > I_{min}$)	$\frac{(I_{max} - I_o)^2 (1 - D_1) T_s}{2(\Delta I_L) C}$	$\frac{D_2 T_S (I_{max} - I_o)^2}{2C I_{max}}$

is given in table 9. The value of capacitor ripple voltage is calculated from ΔI_L and is tabulated in table 9. The value of output ripple voltage is given by

$$\Delta V_o{}^2 = \Delta V_c{}^2 + (\Delta I_C R_c)^2. \tag{15}$$

Depending on the relative magnitude of ΔI_c or ΔV_C, the output ripple voltage ΔV_o is approximated as

$$\Delta V_o = \Delta V_c; \text{ or } \Delta V_o = \Delta I_C \, R_c. \tag{16}$$

5.2 *Harmonic model of boost converter*

In an ideal boost converter, the voltage across the inductor is V_g or (V_g–V_o) or zero; depending on the conduction of switch and diode. In a non-ideal boost converter, the voltage across the inductor reduces from its ideal value by the drop in resistive non-idealities. During ON period of the switch (i.e. $D_1 T_s$), the drop is calculated using the average value of inductor current, obtained from the average model of boost converter. The value of ripple in inductor current is given by the expression, tabulated in table 10.

When the switch is OFF i.e. during $(1-D_1)T_s$ or $D_2 T_s$, the inductor current flows through the diode. The average diode current is equal to the load current (I_0). The ripple in diode current flows through the capacitor.

Under CCM, the minimal value of inductor current is indicated as i_{min}, as shown in figure 8(a). When the load current i_0 is less than i_{min}, the capacitor ripple current is plotted in figure 8(b). From the capacitor ripple current, the ripple in capacitor voltage (ΔV_C) is determined as shown in figure 8(c). The output voltage ripple is given by the sum of resistive drop across R_c and ΔV_C, as plotted in figure 8(d).

Under CCM, when the load current i_o is higher than the minimal value of inductor current i_{min}, the shape of ripple current through the capacitor varies, as shown in figure 9(b). The capacitor

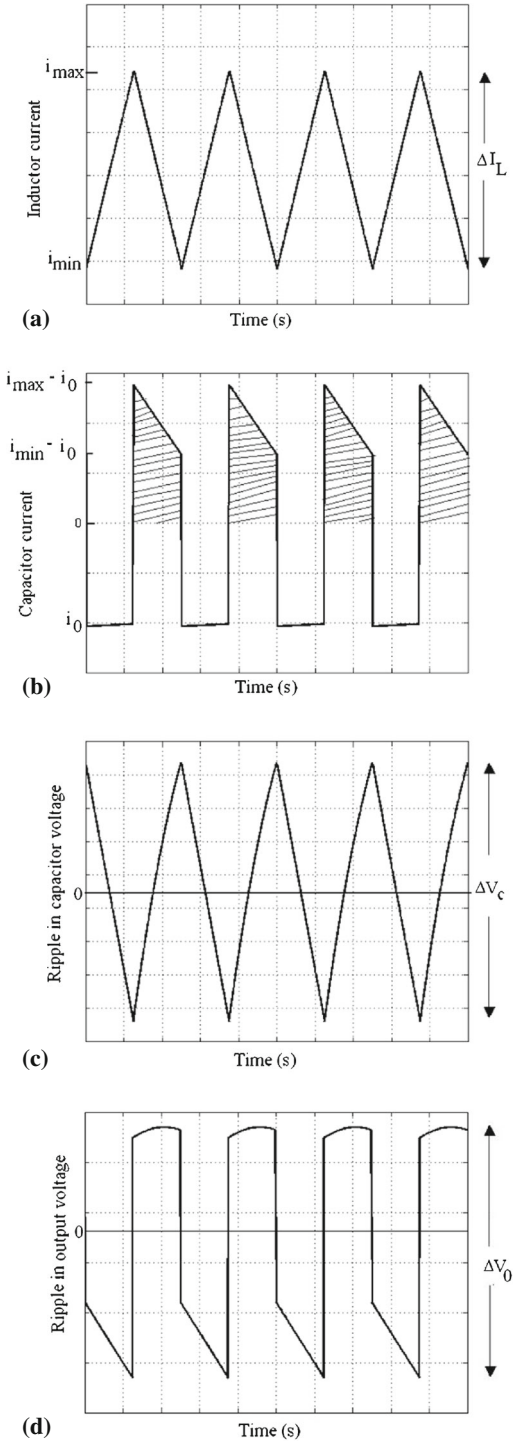

Figure 8. Boost converter under CCM when $i_0 < i_{\min}$ (**a**) inductor current (**b**) capacitor current (**c**) ripple in capacitor voltage (**d**) ripple in output voltage.

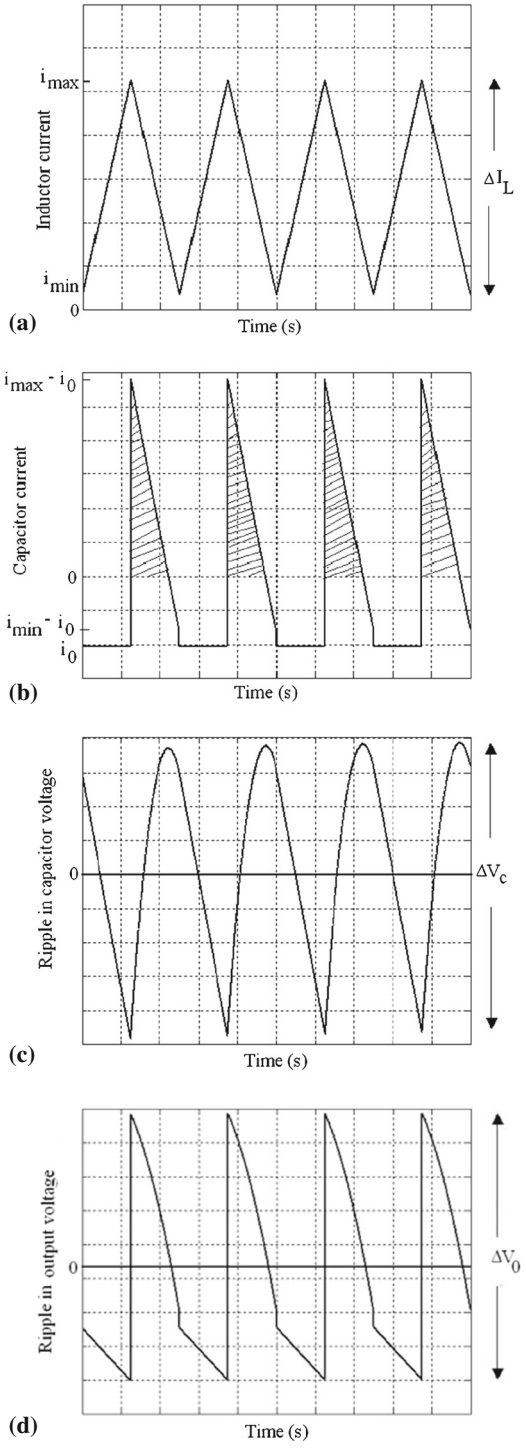

Figure 9. Boost converter under CCM when $i_0 > i_{\min}$ (**a**) inductor current (**b**) capacitor current (**c**) ripple in capacitor voltage (**d**) ripple in output voltage.

ripple voltage and output ripple voltage under this mode of operation is shown in figure 9(c) and 9(d) respectively. Under DCM, the minimal value of inductor current is zero. The capacitor current has the same shape, similar to that shown in figure 9(b).

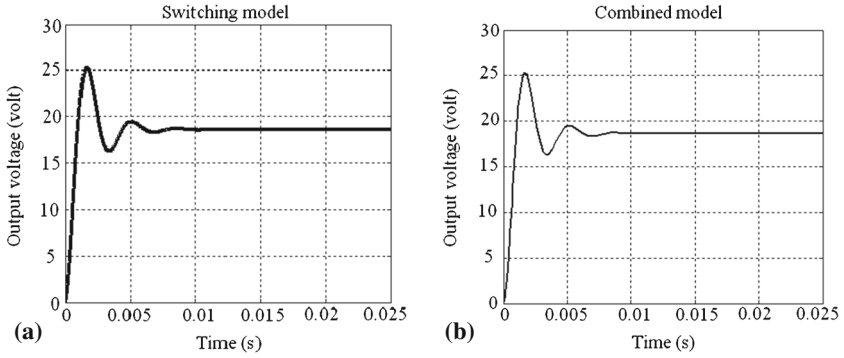

Figure 10. Output voltage of buck converter: $D_1 = 0.53$, $R = 100\Omega$, $V_g = 40$ V (**a**) switching model (**b**) combined model.

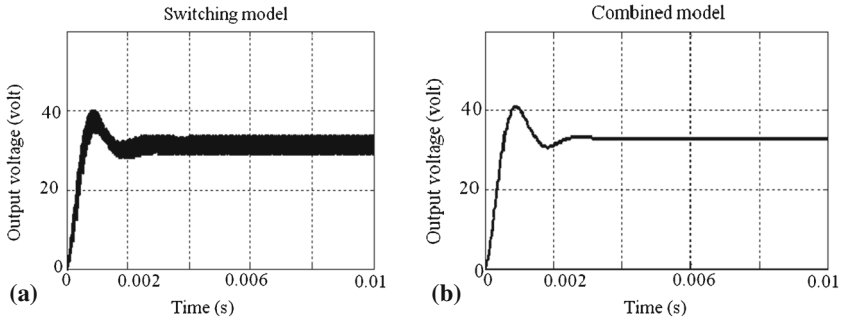

Figure 11. Output voltage of boost converter: $D_1 = 0.48$, $R = 50\Omega$, $V_g = 20$ V (**a**) switching model (**b**) combined model.

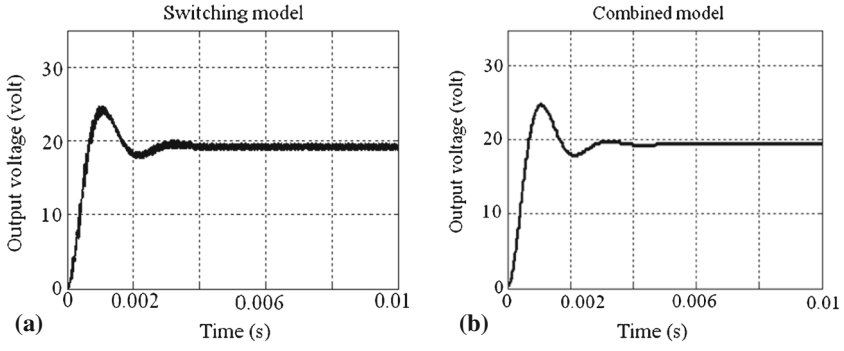

Figure 12. Output voltage of Buck–Boost converter: $D_1 = 0.54$, $R = 100\Omega$, $V_g = 20$ V (**a**) switching model (**b**) combined model.

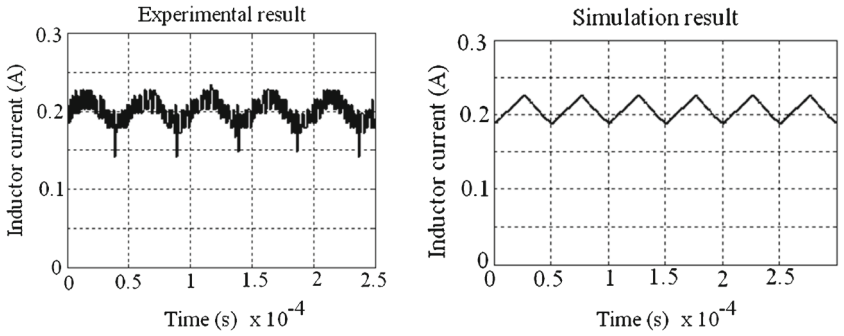

Figure 13. Inductor current of buck converter under CCM: $D_1 = 0.53$, $R = 100\Omega$, $V_g = 40$ V, $f_s = 20$ kHz.

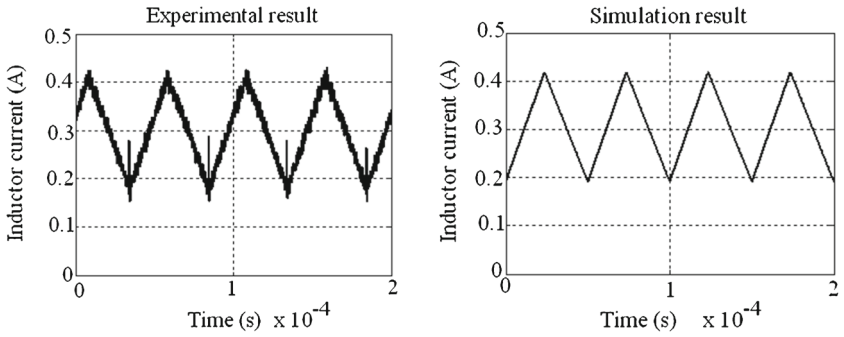

Figure 14. Inductor current of boost converter under CCM: $D_1 = 0.48$, $R = 222\Omega$, $V_g = 20$ V, $f_s = 20$ kHz.

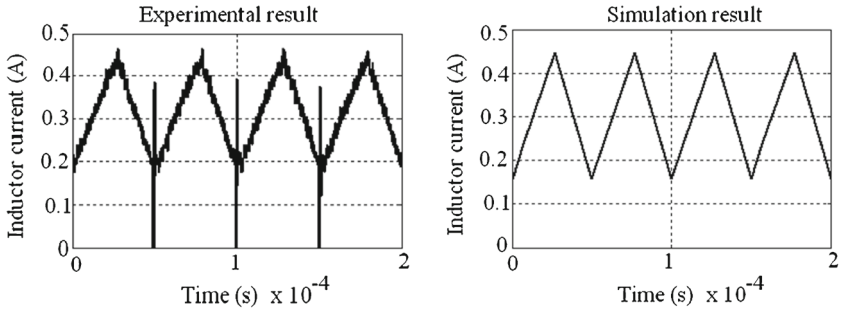

Figure 15. Inductor current of buck–boost converter under CCM: $D_1 = 0.54$, $R = 222\Omega$, $V_g = 20$ V, $f_s = 20$ kHz.

The ripple in capacitor voltage (ΔV_c) is calculated as the time integral of positive value of capacitor current, as shown by dashed lines in figures 8–9. The value of ΔV_c under various operation modes of the boost converter is tabulated in table 10. The ripple in output voltage is determined using (15) and (16).

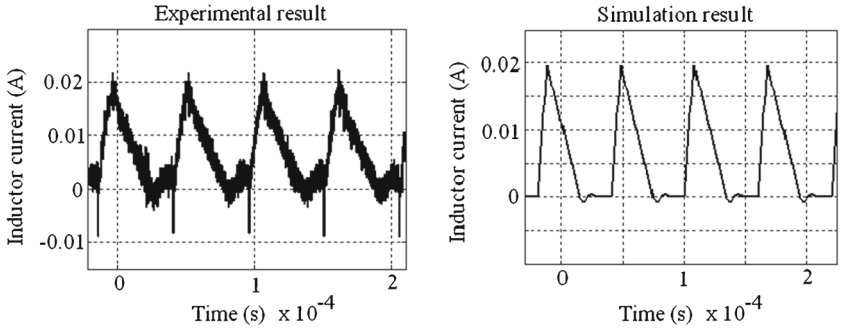

Figure 16. Inductor current of buck converter under DCM: $D_1 = 0.12$, $R = 1,600\Omega$, $V_g = 40$ V, $f_s = 16.8$ kHz.

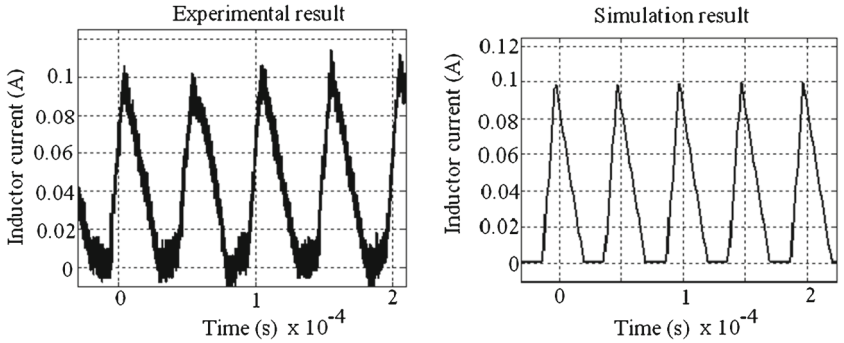

Figure 17. Inductor current of boost converter under DCM: $D_1 = 0.48$, $R = 1,600\Omega$, $V_g = 20$ V, $f_s = 20$ kHz.

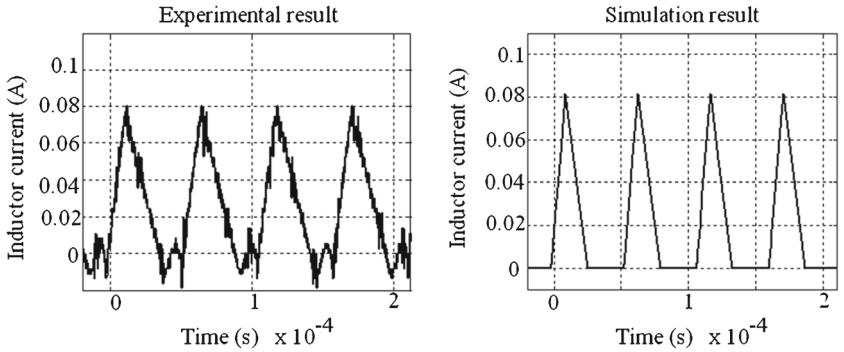

Figure 18. Inductor current of buck–boost converter under DCM: $D_1 = 0.12$, R = 980 Ω, $V_g = 20$ V, $f_s = 18.5$ kHz.

5.3 *Harmonic model of buck–boost converter*

In a buck–boost converter, the inductor current flows through the diode during off-time of active switch. The average diode current flows through the load. The ripple in diode current flows

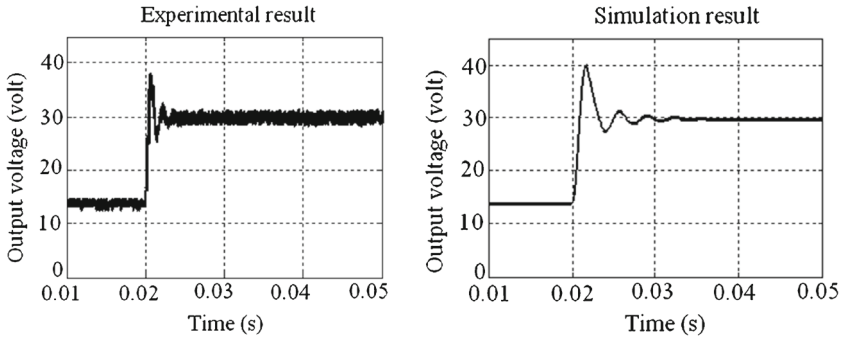

Figure 19. Output voltage transient for buck converter under: $D_1 = 0.36$ to 0.56, $R = 100\Omega$, $V_g = 40$ V, $f_s = 20$ kHz.

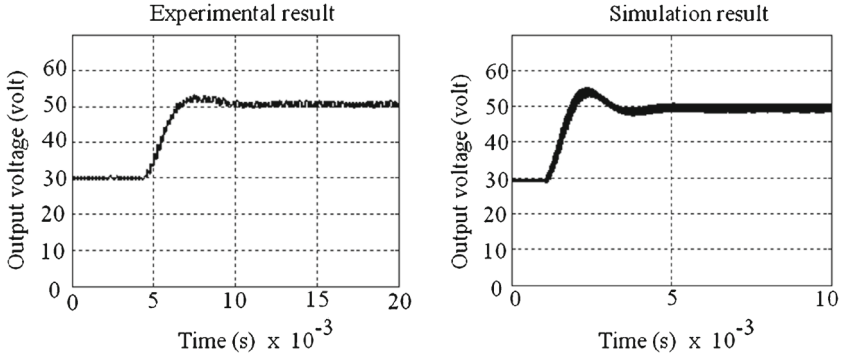

Figure 20. Output voltage of boost converter: $D_1 = 0.36$ to 0.64, $R = 222\Omega$, $V_g = 20$V, $f_s = 20$ kHz.

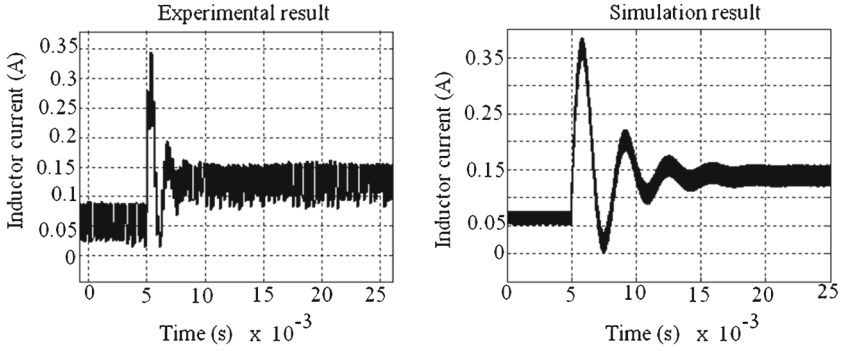

Figure 21. Inductor current in a buck converter for a step change in D_1 from 0.36 to 0.56, $R = 100\Omega$, $V_g = 40$ V, $f_s = 20$ kHz.

through the capacitor. From the perspective of ripple current and voltage, the structure is much similar to that of boost converter. The value of ΔI_L and ΔV_c under various modes of operation of buck–boost converter is tabulated in table 10.

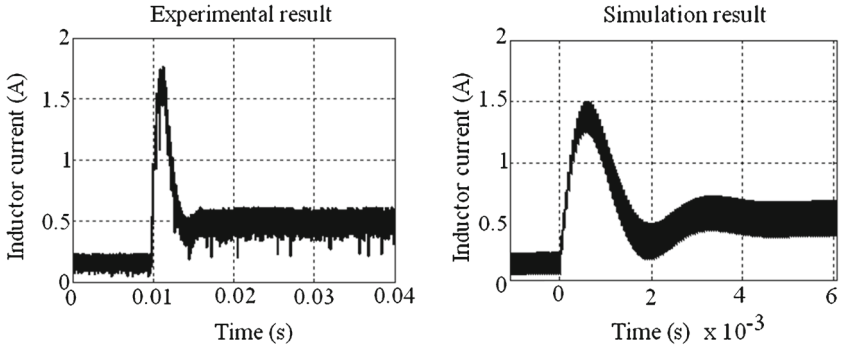

Figure 22. Inductor current in a boost converter for a step change in D_1 from 0.36 to 0.64, $R = 222\Omega$, $V_g = 20$ V, $f_s = 20$ kHz.

Table 11. Comparison of simulation and experimental results from buck converter: $V_g = 40$V.

Parameter	Mode	D_1	R (Ω)	Experimental result	Combined model	Switching model
Output	CCM	0.5	100	20.01	20.35	20.35
voltage (V_o)	DCM	0.2	1,170	27.4	27.67	27.625
Inductor	CCM	0.5	100	0.2	0.203	0.203
current (I_L)	DCM	0.2	1,170	0.038	0.04857	0.036
Inductor ripple	CCM	0.5	100	0.04	0.04	0.04
current (ΔI_L)	DCM	0.2	1,170	0.105	0.106	0.102
Output ripple	CCM	0.5	100	0.06	0.0578	0.058
voltage (ΔV_o)	DCM	0.2	1,170	0.58	0.3585	0.3

Table 12. Comparison of simulation and experimental results from boost converter: $V_g = 20$ V.

Parameter	Mode	D_1	$R(\Omega)$	Experimental result	Combined model	Switching model
Output	CCM	0.48	222	35.62	36.43	36V
voltage (V_o)	DCM	0.2	1,170	27.4	27.67	27.625
Inductor	CCM	0.48	222	0.3	0.3125	0.315
current (I_L)	DCM	0.2	1,170	0.038	0.04857	0.036
Inductor ripple	CCM	0.48	222	0.25	0.2322	0.235
current (ΔI_L)	DCM	0.2	1,170	0.105	0.106	0.102
Output ripple	CCM	0.48	222	1.2	1.52	1.2
voltage (ΔV_o)	DCM	0.2	1,170	0.58	0.3585	0.3

Table 13. Comparison of simulation and experimental results from buck–boost converter: $V_g = 20$ V.

Parameter	Mode	D_1	R (Ω)	Experimental result	Combined model	Switching model
Output	CCM	0.55	222	21.43	21.9	21.9
voltage (V_o)	DCM	0.13	980	7.2	7.22	7.55
Inductor	CCM	0.55	222	0.246	0.22	0.22
current (I_L)	DCM	0.13	980	0.1	0.0103	0.0105
Inductor ripple	CCM	0.55	222	0.21	0.21	0.21
current (ΔI_L)	DCM	0.13	980	0.66	0.052	0.052
Output ripple	CCM	0.55	222	0.8	0.47	0.4
voltage (ΔV_o)	DCM	0.13	980	0.7	0.0542	0.4

Table 14. Comparison of computational time under steady-state condition of converters.

Type	Mode	D_1	R (Ω)	Duration (s)	Switching model (s)	Average model (s)	Combined model (s)
Buck	CCM	0.8	100	0.2	11.53	0.505	0.817
	DCM	0.2	1,610	0.5	29.34	1.479	1.806
Boost	CCM	0.4	222	0.2	9.1	0.479	0.665
	DCM	0.2	1,600	0.5	23.84	1.291	1.321
Buck–Boost	CCM	0.54	222	0.2	14.47	0.528	0.552
	DCM	0.2	1,500	0.5	39.87	1.344	1.688

Table 15. Comparison of computation time among switching, average and combined models under transient conditions for buck converter.

Transition	Mode	Switching model (s)	Average model (s)	Combined model (s)
Step change in D_1 from 0.4 to 0.8; $V_g = 40$ V, $R = 222\ \Omega$	CCM	1.262	0.1062	0.1095
Step change in D_1 from 0.6 to 0.2; $V_g = 40$ V, $R = 222\ \Omega$	CCM	1.305	0.0492	0.084
Step change in D_1 from 0.2 to 0.4; $V_g = 40$ V, $R = 2,500\ \Omega$	DCM	5.641	0.1664	0.276
Step change in D_1 from 0.5 to 0.25; $V_g = 40$ V ,$R = 2,500\ \Omega$	DCM	4.437	0.1293	0.2279
Step change in R from 750 Ω to 150 Ω; $V_g = 40$ V; $D_1 = 0.8$	CCM	4.0511	0.1291	0.1398
Step change in R from 200 Ω to 1,000 Ω; $V_g = 40$ V, $D_1 = 0.8$	CCM	6.4978	0.0458	0.09701
Step change in R from 2,250 Ω to 1,750 Ω; $V_g = 40$ V, $D_1 = 0.2$	DCM	3.582	0.052	0.1121
Step change in R from 1,750 Ω to 2,250 Ω; $V_g = 40$ V, $D_1 = 0.2$	DCM	3.583	0.0512	0.112
Step change in R from 150 Ω to 1,750 Ω; $V_g = 40$ V, $D_1 = 0.2$	CCM to DCM	4.573	0.1403	0.184
Step change in R from 2,500 Ω to 250 Ω; $V_g = 40$ V, $D_1 = 0.4$	DCM to CCM	2.237	1.1312	0.1392
Step change in V_g from 35 V to 45 V; $D_1 = 0.65$, $R = 100\ \Omega$	CCM	1.511	0.0516	0.0794
Step change in V_g from 45V to 35 V; $D_1 = 0.65$, $R = 500\ \Omega$	CCM	2.2602	0.0847	0.0892
Step change in V_g from 45 V to 35 V; $D_1 = 0.2$, $R = 1,600\ \Omega$	DCM	6.769	0.1185	0.1461
Step change in V_g from 35 V to 45 V; $D_1 = 0.2$, $R = 2,500\ \Omega$	DCM	11.0474	0.1318	0.3401

6. Validation of simulation models

The harmonic and average models are combined together and referred as "combined model" in this paper for further discussion. This section discusses the comparison of combined

Table 16. Comparison of computation time among switching, average and combined models under transient conditions for boost converter.

Transition	Mode	Switching model (s)	Average model (s)	Combined model (s)
Step change in D_1 from 0.3 to 0.5; $V_g = 21.4$ V, $R = 105\ \Omega$	CCM	4.537	0.0707	0.177
Step change in D_1 from 0.7 to 0.2; $V_g = 21.4$ V, $R = 105\ \Omega$	CCM	4.863	0.0814	0.101
Step change in R from 105 Ω to 210 Ω; $V_g = 21.4$ V, $D_1 = 0.5$	CCM	4.855	0.077	0.106
Step change in R from 800 Ω to 200 Ω; $V_g = 21.4$ V, $D_1 = 0.5$	CCM	4.818	0.07	0.088
Step change in R from 105 Ω to 1,750 Ω; $V_g = 21.4$ V, $D_1 = 0.5$	CCM to DCM	5.872	0.078	0.0875
Step change in D_1 from 0.3 to 0.5; $V_g = 21.4$ V, $R = 1,750\ \Omega$	DCM	4.761	0.0795	0.2351
Step change in D from 0.5 to 0.2; $V_g = 21.4$ V, $R = 1,750\ \Omega$	DCM	4.97	0.0815	0.2433
Step change in R from 1,750 Ω to 2,000 Ω; $V_g = 21.4$ V, $D_1 = 0.5$	DCM	5.141	0.0396	0.2071
Step change in R from 1,750 Ω to 105 Ω; $V_g = 21.4$ V, $D_1 = 0.5$	DCM to CCM	4.7313	0.0368	0.2627
Step change in V_g from 21.4 V to 25 V; $R = 105\ \Omega$; $D_1 = 0.5$	CCM	4.7157	0.0672	0.2627
Step change in V_g from 21.4 V to 25 V; $R = 1,750\ \Omega$, $D_1 = 0.2$	DCM	4.9078	0.0436	0.1843
Step change in V_g from 25 V to 21.4 V; $R = 105\ \Omega$; $D_1 = 0.5$	CCM	5.339	0.0628	0.0781
Step change in V_g from 25 V to 21.4 V; $R = 1,750\Omega$, $D_1 = 0.2$	DCM	4.604	0.0484	0.2277

model with the switching model in terms of accuracy and also the experimental validation of all the models.

6.1 *Comparison of combined model and switching model*

The combined model gives all the information, as provided by the switching model. To validate this claim, the output from combined model and switching model of various converters are compared in figures 10–12. It is clear from the simulation results that the transient and steady-state values produced by the combined and switching models are similar.

6.2 *Experimental validation*

The accuracy of the models of buck, boost and buck–boost converters are verified by comparing the simulation results with that of the converter hardware. All the experiments were conducted on 20 W laboratory prototypes of various converters, built in lab. The switching frequency (f_s) of the firing signal to the MOSFET switch IRF741 is generated at 20 kHz by PWM generator IC TL494. The output voltage and inductor current of various converters are recorded in the digital

Table 17. Comparison of computation time among switching, average and combined models under transient conditions for buck–boost converter.

Transition	Mode	Switching model (s)	Average model (s)	Combined model (s)
Step change in D_1 from 0.2 to 0.5; $V_g = 20$ V, $R = 195\Omega$	CCM	0.72773	0.01085	0.036695
Step change in D_1 from 0.5 to 0.2; $V_g = 20$ V, $R = 195\ \Omega$	CCM	0.186182	0.012979	0.013756
Step change in D_1 from 0.3 to 0.6; $V_g = 20$ V, $R = 2,000\ \Omega$	DCM	6.351	0.042876	0.087433
Step change in D_1 from 0.75 to 0.25; $V_g = 20$ V, $R = 2,500\ \Omega$	DCM	6.4418	0.098904	0.71078
Step change in R from 150 Ω to 250 Ω; $V_g = 20$ V, $D_1 = 0.6$	CCM	1.341	0.025946	0.029823
Step change in R from 350 Ω to 150 Ω; $V_g = 20$ V, $D_1 = 0.5$	CCM	0.44658	0.015458	0.039702
Step change in R from 1,000 Ω to 1,500 Ω; $V_g = 20$ V, $D_1 = 0.3$	DCM	3.6676	0.021591	0.024907
Step change in R from 1,750 Ω to 1,250 Ω; $V_g = 20$ V, $D_1 = 0.35$	DCM	3.1622	0.027203	0.03116
Step change in R from 250 Ω to 1,250 Ω; $V_g = 20$ V, $D_1 = 0.3$	CCM to DCM	13.9611	0.062899	0.096064
Step change in R from 2,500 Ω to 200 Ω; $V_g = 20$ V, $D_1 = 0.55$	DCM to CCM	1.8534	0. 143407	0.14738
Step change in V_g from 18 V to 25 V; $R = 150\ \Omega$, $D_1 = 0.5$	CCM	0.34463	0.018372	0.082372
Step change in V_g from 18 V to 25 V; $R = 1,500\ \Omega$, $D_1 = 0.3$	DCM	5.56905	0.046704	0.054054
Step change inV_g from 22 V to 15 V; $R = 2,500\ \Omega$, $D_1 = 0.4$	DCM	0.87823	0.011518	0.081345

storage oscilloscope. The simulation results from switching model and experimental results are compared for validating the models. It is also clear from the previous discussions that the simulation results from combined and switching model tally with each other. Hence, it is reasonable to compare the results from switching model and experiment for verification of accuracy of the model.

The steady-state inductor current under CCM and DCM operation of the converters is compared in figures 13–18. The dynamic operation of the converters under change in duty cycle is compared in figures 19 and 20. Inductor current transient with change in duty cycle is compared in figures 21 and 22. It is clear from the results that the model is an accurate representation of the actual converter. To emphasize the accuracy of the models, the quantitative comparison of the results from switching model, combined model and experiment is provided in tables 11–13.

7. Analysis of computational time

The switching, average and combined models of buck, boost and buck–boost converters are simulated in MATLAB with a fixed step ODE solver. The step time for the simulation of switching,

average and combined models of converters are 1e−7, 1e−5 and 1e−5 s respectively. The computational time for the converters to reach the steady-state operating condition is tabulated in table 14. The computation time of converters under transient conditions is listed in tables 15–17. From the tabulated value of computational time, it is clear that the average and combined models consume minimum time, as compared to that of switching model. During off-line simulation of dc–dc converters, the average and combined model can be satisfactorily used instead of the conventional switching model.

8. Conclusion

The switching, average and combined (average + harmonic) models of buck, boost and buck–boost converters, including the non-idealities of the components, are developed. The models are simulated in off-line simulation environment with a fixed time-step. The time-step required for the switching model is much lower than that of the average and combined models. The computation time required by various models under steady-state and transient operating conditions of the converters are determined. From the obtained results, it is clear that the average and combined models take minimum computation time. The prototype of all the converters is built in the lab and the accuracy of the models is verified by comparing the simulation results with the hardware results. The models described in this paper are accurate and can mimic the behavior of the converters under steady-state and transient conditions. The detailed analysis of the models of the converters under various operating conditions proves that the combined model can replace the switching model of dc–dc converters, without any loss of accuracy.

Acknowledgement

This work was supported by the Department of Heavy Industry, Government of India, under the project entitled "Development of offline and real time simulators for electric vehicle/hybrid electric vehicle systems".

References

Badstuebner U, Biela J and Kolar J W 2010 Design of an 99%-efficient, 5 kW, phase-shift PWM dc-dc converter for telecom applications. In: *Twenty-Fifth Annual IEEE Applied Power Electronics Conference and Exposition*, pp. 773–780

Bellur D M, Dayton O H and Kazimierczuk 2007 DC-DC converters for electric vehicle applications. In: *Electrical Insulation Conference and Electrical Manufacturing Expo*, pp. 286–293

Chung I, Liu W, Andrus M, Schoder K, Leng S, Cartes D A and Steurer M 2009 Integration of a bi-directional dc-dc converter model in to a large-scale system simulation of a ship board MVDC power system. In: *IEEE Electric Ship Technology Symposium*, pp. 318–325

Emadi A, Williamson S S and Khaligh A 2006 Power electronics intensive solutions for advanced electric, hybrid electric and fuel cell vehicular power systems. *IEEE Trans. Power Electron.* 21(3): 567–577

Fang C 2011 Unified discrete-time modeling of buck converter in discontinuous mode. *IEEE Trans. Power Electron.* 26(8): 2335–2342

Hwang T and Park S 2012 Seamless boost converter control under the critical boundary condition for a fuel cell power conditioning system. *IEEE Trans. Power Electron.* 27(8): 3616–3626

Jalla M M, Emadi A, Williamson G A and Fahimi B 2004 Real time state estimation of multi- converter more electric ship power systems using the generalized state space averaging method. In: *30th Annual conference of IEEE Industrial Electronics Society*, pp. 1514–1519

Khan I A 1994 DC-to-DC converters for electric and hybrid electric vehicles. In: *IEEE Proceedings of the Power Electronics in Transportation*, pp. 113–122

Krein P T, Bentsman J, Bass R M and Lesieutre B C 1989 On the use of averaging for the analysis of power electronic systems. In: *IEEE Power Electronics Specialists Conference*, pp. 463–467

Lehman B and Bass R M 1994 Recently developed averaging theory applied to power electronic systems. In: *IEEE Proceedings of the American Control Conference*, pp. 1563–1567

Merdassi A, Gerbaud L and Bacha S 2008 A new automatic average modeling tool for power electronic systems. In: *IEEE Power Electronics Specialists Conference*, pp. 3425–3431

Mohan N, Undeland T M and Robbins W P 2007 *Power electronics: Converters, applications, and design*. Wiley student edition, New Delhi, India, pp. 322–341

Patil M B, Ranganathan V T and Ramanarayanan V 2009 *Simulation of power electronic circuits*. Narosa, New Delhi, India, pp. 17.9–17.19

Pedicini C, Iannelli L and Vasca F 2012 The averaging method for control design and stability analysis of practical switched systems. In: *IEEE International Conference on Control Applications*, pp. 1285–1290

Ren Y, Kang W and Qian Z 2000 A novel average model for single switch buck-boost dc-dc converter. In: *Power Electronics and Motion Control Conference*, pp. 436–439

Sanders S R, Noworolski J M, Liu X Z and Verghese G C 1990 Generalized averaging method for power conversion circuits. In: *IEEE Proceedings of Power Electronics Specialists Conference*, pp. 333–340

Saritha B, Pandey V and Narayanan G 2013 Computationally efficient model for simulation of boost converter. In: *National Power Electronics Conference*, IIT Kanpur, India

Vuthchhay E and Bunlaksananusorn C 2008 Dynamic modeling of a zeta converter with state- space averaging technique. In: *5th International Conference on Electrical Engineering/Electronics, Computer, Telecommunications and Information Technology*. 2: 969–972

Waffler S and Kolar J W 2009 A novel low-loss modulation strategy for high-power bidirectional buck boost converters. *IEEE Trans. Power Electron.* 24(6): 1589–1599

Williamson S S, Lukic S M and Emadi A 2006 Comprehensive drive train efficiency analysis of hybrid electric and fuel cell vehicles based on motor controller efficiency modeling. *IEEE Trans. Power Electron.* 21(3): 730–740

Zahedi B and Norum L E 2013 Modeling and simulation of all electric ships with low-voltage dc hybrid power systems. *IEEE Trans. Power Electron.* 28(10): 4525–4537